
MagNet: A Magnetic Neural Network for Directed Graphs

Xitong Zhang¹ Nathan Brugnone^{1,2} Michael Perlmuter^{*3} Matthew Hirn^{*1,4,5}

Abstract

The prevalence of graph-based data has spurred the rapid development of graph neural networks (GNNs) and related machine learning algorithms. Yet, despite the many data sets naturally modeled as directed graphs, including citation, website, and traffic networks, the vast majority of this research focuses on undirected graphs. In this paper, we propose *MagNet*, a spectral GNN for directed graphs based on a complex Hermitian matrix known as the magnetic Laplacian. This matrix encodes undirected geometric structure in the magnitude of its entries and directional information in the phase of its entries. A “charge” parameter attunes spectral information to variation among directed cycles. We show that *MagNet*’s performance exceeds other spectral GNNs on directed graph node classification and link prediction tasks for a variety of datasets and exceeds commonly used spatial GNNs on a majority of such. The underlying principles of *MagNet* are such that it can be adapted to other spectral GNN architectures.

1. Introduction

Endowing a collection of objects with a graph structure allows one to encode pairwise relationships among its elements. These relations often possess a natural notion of direction. For example, the WebKB dataset, shown in Figure 1, contains a list of university websites with associated hyperlinks. In this context, one website might link to a second without a reciprocal link to the first. Such datasets

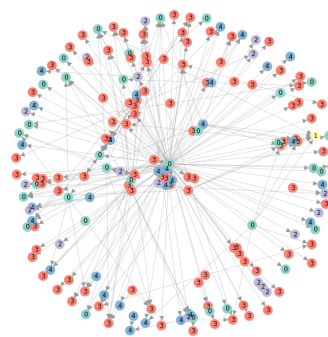


Figure 1. Visualization of WebKB-Cornell. Vertex colors denote different classes.

are naturally modeled by *directed graphs*. In this paper, we introduce *MagNet*, a graph convolutional neural network for directed graphs based on the magnetic Laplacian.

Most graph neural networks fall into one of two families, *spectral networks* or *spatial networks*. Spatial methods define graph convolution as a localized averaging operation with iteratively learned weights. Spectral networks, on the other hand, define convolution on graphs via the eigendecomposition of the (normalized) graph Laplacian. The eigenvectors of the graph Laplacian assume the role of Fourier modes, and convolution is defined as entrywise multiplication in the Fourier basis. For a comprehensive review of both spatial and spectral networks, we refer the reader to Zhou et al. (2018) and Wu et al. (2020).

Many common spatial graph CNNs have natural extensions to directed graphs. However, it is common among these methods to preprocess the data by symmetrizing the adjacency matrix, effectively creating an undirected graph. For example, Veličković et al. (2018) explicitly note that their network is well-defined on directed and undirected graphs, yet their experiments treat all citation networks as undirected for improved performance.

Extending spectral methods to directed graphs is not straightforward since the adjacency matrix is asymmetric and, thus, there is no obvious way to define a symmetric Laplacian with a full set of real eigenvalues. We overcome this challenge by constructing a network based on the magnetic

^{*}Equal contribution ¹Michigan State University, Department of Computational Mathematics, Science and Engineering, East Lansing, Michigan, United States ²Michigan State University, Department of Community Sustainability, East Lansing, Michigan, United States ³University of California, Los Angeles, Department of Mathematics, Los Angeles, California, United States ⁴Michigan State University, Department of Mathematics, East Lansing, Michigan, United States ⁵Michigan State University, Center for Quantum Computing, Science and Engineering, East Lansing, Michigan, United States. Correspondence to: Matthew Hirn <mhirn@msu.edu>.

Laplacian $\mathbf{L}^{(q)}$ defined in Section 2. Unlike the directed graph Laplacians constructed in works such as Ma et al. (2019), Monti et al. (2018), Tong et al. (2020b), and Tong et al. (2020a), the magnetic Laplacian is not a real-valued symmetric matrix. Instead, it is a complex-valued *Hermitian* matrix that encodes the fundamentally asymmetric nature of a directed graph via the complex phase of its entries.

Since $\mathbf{L}^{(q)}$ is Hermitian, the spectral theorem implies it has an orthonormal basis of complex eigenvectors corresponding to real eigenvalues. Setting $q = 0$ is effectively equivalent to symmetrizing the adjacency matrix and no importance is given to directional information in this case. When $q = .25$, on the other hand, we have that $\mathbf{L}^{(.25)}(u, v) = -\mathbf{L}^{(.25)}(v, u)$ whenever there is a directed edge from u to v but not from v to u . By learning the appropriate value of q , we allow the network to adaptively incorporate directed information based upon the graph and the task.

In Section 3, we show how the networks constructed in Bruna et al. (2014), Defferrard et al. (2016), and Kipf & Welling (2016) can be adapted to the directed graph setting by incorporating the magnetic Laplacian. We note that when $q = 0$, we effectively recover the networks constructed in those previous works. Therefore, we generalize these networks in a way that is suitable for directed graphs. In fact, this is a general principle not specific to any particular choice of spectral network architecture, and indeed could be applied to other spectral networks as well.

In Section 4, we summarize related work with a focus on neural networks designed for directed graphs and other papers studying the magnetic Laplacian. In Section 5, we apply our network to node classification and link prediction tasks in directed networks. We compare against several spectral and spatial methods as well as two networks designed for directed graphs. We find that our network obtains the best performance on six out of eight node-classification tasks and seven out of nine link-prediction tasks.

2. The Magnetic Laplacian

Spectral graph theory has been remarkably successful in relating local and global characteristics of undirected graphs to properties of eigenvectors and eigenvalues of graph Laplacians. For example, the tasks of optimal graph partitioning, sparsification, clustering, and embedding may be approximated, subject to local measures of density, by eigenvectors corresponding to small eigenvalues of various graph Laplacians (see, e.g., Chung & Graham (1997), Shi & Malik (1997), Belkin & Niyogi (2003), Spielman & Teng (2004), and Coifman & Lafon (2006)). Similarly, the graph signal processing research community leverages the full set of eigenvectors to extend the Fourier transform to these

structures (Ortega et al., 2018). Numerous papers have, furthermore, shown that this eigendecomposition can be used to define convolutional neural networks on graphs. Several of these works, Bruna et al. (2014), Defferrard et al. (2016), and Kipf & Welling (2016), are discussed in Section 3. In this section, we provide the background needed to extend these constructions to directed graphs via the magnetic Laplacian.

We let $G = (V, E)$ be a directed graph where V is a set of N vertices and $E \subseteq V \times V$ is a set of directed edges. If $(u, v) \in E$, then we say there is an edge from u to v . For the sake of simplicity, we will focus on the case where the graph is unweighted and has no self-loops, i.e., $(v, v) \notin E$, but our methods have natural extensions to graphs with self-loops and/or weighted edges. If both $(u, v) \in E$ and $(v, u) \in E$, then one may consider this pair of directed edges as a single undirected edge. Graphs with both directed and undirected edges are sometimes referred to as mixed graphs, but this distinction is not of great import here.

A directed graph can be described by an adjacency matrix

$$\mathbf{A}(u, v) := \begin{cases} 1 & (u, v) \in E \\ 0 & (u, v) \notin E \end{cases}.$$

Unless G is undirected, \mathbf{A} is not symmetric, and, indeed, this is the key technical challenge in extending spectral graph neural networks to directed graphs. In the undirected case, where the adjacency matrix \mathbf{A} is symmetric, the (unnormalized) graph Laplacian can be defined by $\mathbf{L} = \mathbf{D} - \mathbf{A}$, where \mathbf{D} is a diagonal degree matrix. It is well-known that \mathbf{L} is a symmetric, positive-semidefinite matrix and therefore has an orthonormal basis of eigenvectors associated with non-negative eigenvalues. However, in the case where \mathbf{A} is asymmetric, direct attempts to define the Laplacian this way typically yield complex eigenvalues. This impedes the straight-forward extension of classical methods of spectral graph theory and graph signal processing to directed graphs.

In order to use spectral methods while still capturing the fundamentally asymmetric nature of a directed graph, we construct a Hermitian adjacency matrix and associated normalized and unnormalized Laplacians. To do so, define the symmetrized adjacency matrix,

$$\mathbf{A}_s(u, v) := \frac{1}{2}(\mathbf{A}(u, v) + \mathbf{A}(v, u)),$$

for $1 \leq u, v \leq N$, and the diagonal degree matrix by

$$\mathbf{D}_s(u, u) := \sum_{v \in V} \mathbf{A}_s(u, v),$$

with $\mathbf{D}_s(u, v) = 0$ for $u \neq v$. We capture directional information via a phase matrix, $\Theta^{(q)}$, defined for $q \geq 0$ by

$$\Theta^{(q)}(u, v) := 2\pi q(\mathbf{A}(u, v) - \mathbf{A}(v, u)),$$

and define $\exp(i\Theta^{(q)})$ component-wise by

$$\exp(i\Theta^{(q)})(u, v) := \exp(i\Theta^{(q)}(u, v)). \quad (1)$$

We define the complex Hermitian adjacency matrix $\mathbf{H}^{(q)}$ by

$$\mathbf{H}^{(q)} := \mathbf{A}_s \odot \exp(i\Theta^{(q)}),$$

where \odot denotes componentwise multiplication. By construction, $\Theta^{(q)}$ is skew-symmetric and so $\mathbf{H}^{(q)}$ is Hermitian.

When $q = 0$, we have $\Theta^{(0)} = 0$ and so $\mathbf{H}^{(0)} = \mathbf{A}_s$. This effectively corresponds to treating the graph as undirected. For $q \neq 0$, the complex phase of $\mathbf{H}^{(q)}$ encodes the direction of each edge. For example, if there is an edge from u to v but not an edge from v to u we have

$$\mathbf{H}^{(q)}(u, v) = \frac{i}{2} = -\mathbf{H}^{(q)}(v, u).$$

We define the unnormalized magnetic Laplacian by

$$\mathbf{L}_U^{(q)} := \mathbf{D}_s - \mathbf{H}^{(q)} = \mathbf{D}_s - \mathbf{A}_s \odot \exp(i\Theta^{(q)}), \quad (2)$$

and the normalized magnetic Laplacian by

$$\mathbf{L}_N^{(q)} := \mathbf{I} - \left(\mathbf{D}_s^{-1/2} \mathbf{A}_s \mathbf{D}_s^{-1/2} \right) \odot \exp(i\Theta^{(q)}). \quad (3)$$

Note that when G is undirected, $\mathbf{L}_U^{(q)}$ and $\mathbf{L}_N^{(q)}$ reduce to the standard undirected Laplacians.

$\mathbf{L}_U^{(q)}$ and $\mathbf{L}_N^{(q)}$ are Hermitian and positive-semidefinite, and are, therefore, diagonalized by a orthonormal basis of complex eigenvectors $\mathbf{u}_1, \dots, \mathbf{u}_N$ associated to real, nonnegative eigenvalues $\lambda_1, \dots, \lambda_N$. In matrix form, we may write,

$$\mathbf{L}_U^{(q)} = \mathbf{U}\Lambda\mathbf{U}^\dagger,$$

where \mathbf{U} is the $N \times N$ matrix whose k -th column is \mathbf{u}_k , Λ is the diagonal matrix with $\Lambda(k, k) = \lambda_k$, and \mathbf{U}^\dagger is the conjugate transpose of \mathbf{U} (a similar formula holds for $\mathbf{L}_N^{(q)}$). In certain cases, as Examples 1 and 2 demonstrate, the magnetic Laplacian may concentrate directional information in either its eigenvectors or eigenvalues, rather than both. For the directed star, Example 1, directional information is concentrated within the eigenvectors. In the case of the directed cycle, Example 2, it is relegated to the spectrum.

Example 1. Let $G^{(\text{in})}$ and $G^{(\text{out})}$ be the directed star graphs with vertices $V = \{1, \dots, N\}$ and edges pointing in/out to the central vertex, respectively, as shown in Figure 2. Then the eigenvalues of $\mathbf{L}_U^{(q, \text{in})}$, the unnormalized magnetic Laplacian on G^{in} , are given by $\lambda_1^{\text{in}} = 0$, $\lambda_k^{\text{in}} = 1/2$ for $2 \leq k \leq N-1$, and $\lambda_N^{\text{in}} = N/2$. If we let $v = 1$ be the central vertex, the corresponding eigenvectors are given by $\mathbf{u}_1^{\text{in}}(1) = e^{2\pi i q}$, $\mathbf{u}_1^{\text{in}}(n) = 1, 2 \leq n \leq N$; $\mathbf{u}_k^{\text{in}} = \delta_k - \delta_{k+1}, 2 \leq k \leq N-1$; and $\mathbf{u}_N^{\text{in}}(1) = -e^{2\pi i q}$,

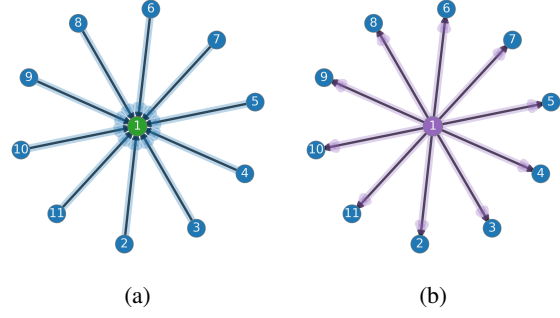


Figure 2. Directed stars (a) $G^{(\text{in})}$, and (b) $G^{(\text{out})}$, with eigenvectors $\mathbf{u}_1^{(\text{in})}$ and $\mathbf{u}_1^{(\text{out})}$ taking values $\mathbf{u}_1^{(\text{in})}(1) = e^{2\pi i q} = \mathbf{u}_1^{(\text{out})}(1)$; edge color corresponds with base node of edge

$\mathbf{u}_N^{\text{in}}(n) = 1/(N-1), 2 \leq n \leq N$. As the phase matrices satisfy $\Theta^{(q, \text{in})} = -\Theta^{(q, \text{out})}$, the associated magnetic Laplacians satisfy $\mathbf{L}_U^{(q, \text{in})}(u, v) = \overline{\mathbf{L}_U^{(q, \text{out})}(u, v)}$. Since these matrices are Hermitian, corresponding eigenvalue-eigenvector pairs satisfy $\lambda_k^{\text{in}} = \lambda_k^{\text{out}}$, and $\mathbf{u}_k^{\text{in}} = \overline{\mathbf{u}_k^{\text{out}}}$. Hence, \mathbf{u}_1^{in} and $\mathbf{u}_1^{\text{out}}$ identify the central vertex, and it is the sign of their imaginary parts at this vertex that identifies whether it is a source or a sink. On the other hand, the eigenvalues give no directional information.

Example 2. By contrast, let G be the directed cycle. Then, analogous to the classical discrete Fourier transform, $\mathbf{L}_U^{(q)}$ is diagonalized in a basis of complex sinusoids with $\mathbf{u}_k(n) = e^{(2\pi i k n)/N}$, independent of q . Therefore, unlike Example 1, directional information is concentrated in the eigenvalues, which in this case are

$$\lambda_k = 1 - \cos\left(2\pi\left(\frac{k}{N} + q\right)\right), \quad 1 \leq k \leq N.$$

Taken together, the star and cycle graphs illustrate extreme cases and suggest the need to incorporate information from both the eigenvectors and eigenvalues for general directed graphs. In Section 3, we will introduce MagNet, a network designed to leverage this spectral information.

3. MagNet

Most graph neural network architectures can be described as being either *spectral* or *spatial*. Spatial networks such as Veličković et al. (2018), Hamilton et al. (2017), Atwood & Towsley (2016), and Duvenaud et al. (2015), typically extend convolution to graphs by performing a weighted average of features over localized neighborhoods $\mathcal{N}_u(v) = \{v : (u, v) \in E\}$. These neighborhoods are well-defined even when E is not assumed to be symmetric, so spatial methods typically have natural extensions to directed graphs. On the other hand, such methods may also use

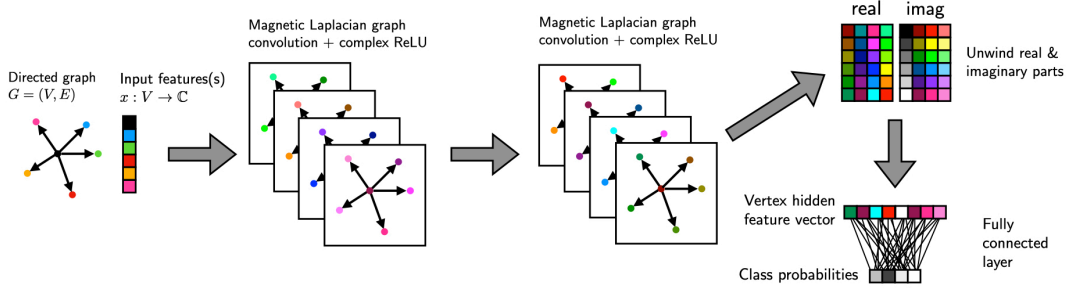


Figure 3. MagNet applied to node classification. After two complex-valued convolutional layers, we unwind the real and imaginary parts of our feature matrix and apply a fully connected layer consisting of a linear transform followed by softmax.

the symmetrized adjacency matrix, but they cannot learn to balance information between these two approaches.

In this section, we show how to extend spectral methods to directed graphs using the magnetic Laplacian introduced in Section 2. Given a graph neural network architecture depending on the graph Laplacian, we may introduce a corresponding method naturally suited for directed graphs by replacing the Laplacian with the magnetic Laplacian and making suitable adjustments to account for the the complex-valued magnetic Laplacian. To highlight the flexibility of our approach, we show how three spectral graph neural network architectures can be adapted to incorporate the magnetic Laplacian. Each of these methods uses a multilayered architecture consisting of convolutions and pointwise activation functions. The principal difference is the class of convolutional filters they consider.

3.1. Spectral Convolution via the Magnetic Laplacian

In this section, we allow $\mathbf{L}^{(q)}$ to be either the normalized or unnormalized magnetic Laplacian introduced in Section 2 on a directed graph $G = (V, E)$, $|V| = N$. We define the directed graph Fourier transform for a signal $\mathbf{x}: V \rightarrow \mathbb{C}$ by $\hat{\mathbf{x}} = \mathbf{U}^\dagger \mathbf{x}$, so that

$$\hat{\mathbf{x}}(k) = \langle \mathbf{x}, \mathbf{u}_k \rangle.$$

We regard the eigenvectors $\mathbf{u}_1, \dots, \mathbf{u}_N$ as the generalizations of discrete Fourier modes to directed graphs. Since \mathbf{U} is unitary, we have the Fourier inversion formula

$$\mathbf{x} = \mathbf{U} \hat{\mathbf{x}} = \sum_{k=1}^N \hat{\mathbf{x}}(k) \mathbf{u}_k. \quad (4)$$

In Euclidean space, convolution corresponds to pointwise multiplication in the Fourier basis. This motivates us to define the convolution of \mathbf{x} with a filter \mathbf{y} in the Fourier domain by $\widehat{\mathbf{y} * \mathbf{x}}(k) = \hat{\mathbf{y}}(k) \hat{\mathbf{x}}(k)$. By (4) this implies

$$\mathbf{y} * \mathbf{x} = \mathbf{U} \text{Diag}(\hat{\mathbf{y}}) \hat{\mathbf{x}} = (\mathbf{U} \text{Diag}(\hat{\mathbf{y}}) \mathbf{U}^\dagger) \mathbf{x}.$$

Therefore, we say \mathbf{Y} is a convolution matrix if

$$\mathbf{Y} = \mathbf{U} \Sigma \mathbf{U}^\dagger, \quad (5)$$

for some diagonal matrix Σ . This is the class of graph convolution matrices considered in Bruna et al. (2014), but adapted for the complex-valued magnetic Laplacian.

Next, following work by Defferrard et al. (2016) and Kipf & Welling (2016), we show that a magnetic spectral network can be implemented in the spatial domain via polynomials of the magnetic Laplacian. This effectively corresponds to restricting the class of Σ considered in (5) by requiring that Σ is a polynomial of Λ . This reduces the number of trainable parameters to prevent overfitting and avoids explicit diagonalization of the Laplacian which is expensive for large graphs. Moreover, Levie et al. (2019) shows that having Σ be a smooth function of Λ improves stability to perturbations. This idea was previously applied to the graph wavelet transform by Hammond et al. (2011).

As in Defferrard et al. (2016), we define a normalized eigenvalue matrix, with entries in $[-1, 1]$, by $\tilde{\Lambda} = \frac{2}{\lambda_{\max}} \Lambda - \mathbf{I}$ and assume that

$$\Sigma = \sum_{k=0}^K \theta_k T_k(\tilde{\Lambda}),$$

for some real-valued $\theta_1, \dots, \theta_k$, where for $k \geq 0$, T_k is the Chebyshev polynomial defined by $T_0(x) = 1$, $T_1(x) = x$, and $T_k(x) = 2xT_{k-1}(x) + T_{k-2}(x)$ for $k \geq 2$. One can use the fact that $(\mathbf{U} \tilde{\Lambda} \mathbf{U}^\dagger)^k = \mathbf{U} \tilde{\Lambda}^k \mathbf{U}^\dagger$ to see

$$\mathbf{Y} \mathbf{x} = \mathbf{U} \sum_{k=0}^K \theta_k T_k(\tilde{\Lambda}) \mathbf{U}^\dagger \mathbf{x} = \sum_{k=0}^K \theta_k T_k(\tilde{\mathbf{L}}) \mathbf{x}, \quad (6)$$

where, analogous to $\tilde{\Lambda}$, we define $\tilde{\mathbf{L}}^{(q)} := \frac{2}{\lambda_{\max}} \mathbf{L}^{(q)} - \mathbf{I}$.

To obtain a network similar to Kipf & Welling (2016), we may set $K = 1$, assume that $\mathbf{L}^{(q)}$ is the normalized magnetic Laplacian, approximate $\lambda_{\max} \approx 2$, and set $\theta_1 = -\theta_0$. With these assumptions we obtain,

$$\mathbf{Y} \mathbf{x} = \theta_0 (\mathbf{I} + (\mathbf{D}_s^{-1/2} \mathbf{A}_s \mathbf{D}_s^{-1/2}) \odot \exp(i \Theta^{(q)})) \mathbf{x}.$$

In Kipf & Welling (2016), the authors apply a renormalization trick to overcome instabilities arising from vanishing/exploding gradients. Similarly, we may substitute $(\mathbf{I} + (\mathbf{D}_s^{-1/2} \mathbf{A}_s \mathbf{D}_s^{-1/2}) \odot \exp(i\Theta^{(q)})) \rightarrow \tilde{\mathbf{D}}_s^{-1/2} \tilde{\mathbf{A}}_s \tilde{\mathbf{D}}_s^{-1/2} \exp(i\Theta^{(q)})$, to obtain

$$\mathbf{Y}\mathbf{x} = \theta_0 \tilde{\mathbf{D}}_s^{-1/2} \tilde{\mathbf{A}}_s \tilde{\mathbf{D}}_s^{-1/2} \odot \exp(i\Theta^{(q)}), \quad (7)$$

where $\tilde{\mathbf{A}}_s = \mathbf{A}_s + \mathbf{I}$ and $\tilde{\mathbf{D}}_s(i, i) = \sum_j \tilde{\mathbf{A}}_s(i, j)$.

3.2. The MagNet Architecture

We now use the spectral convolutions introduced in the previous subsection to define our network. Let L be the number of convolution layers in our network, and let $\mathbf{X}^{(0)}$ be an $N \times F_0$ input feature matrix with columns $\mathbf{x}_1^{(0)}, \dots, \mathbf{x}_{F_0}^{(0)}$. In other words, we have F_0 input features, each of which corresponds to a signal on the vertices of G .

Since we have complex-valued filters, we replace the standard ReLU activation with a complex version defined by

$$\sigma(z) = \begin{cases} z & \text{if } -\pi/2 \leq \arg(z) < \pi/2 \\ 0 & \text{otherwise} \end{cases},$$

where $\arg(z)$ is the complex argument of $z \in \mathbb{C}$.

Let F_ℓ be the number of channels in layer ℓ . For $1 \leq \ell \leq L$, $1 \leq i \leq F_{\ell-1}$, and $1 \leq j \leq F_\ell$, let $\mathbf{Y}_{ij}^{(\ell)}$ be a convolution matrix defined in the sense of either (5), (6), or (7). To obtain the layer ℓ channels from the layer $\ell - 1$ channels, we define for $1 \leq \ell \leq L$ the matrix $\mathbf{X}^{(\ell)}$ with columns $\mathbf{x}_1^{(\ell)}, \dots, \mathbf{x}_{F_\ell}^{(\ell)}$ as:

$$\mathbf{x}_j^{(\ell)} = \sigma \left(\sum_{i=1}^{F_{\ell-1}} \mathbf{Y}_{ij}^{(\ell)} \mathbf{x}_i^{(\ell-1)} \right). \quad (8)$$

In matrix form we write

$$\mathbf{X}^{(\ell)} = \mathbf{Z}^{(\ell)} \left(\mathbf{X}^{(\ell-1)} \right),$$

where $\mathbf{Z}^{(\ell)}$ is a hidden layer of the form (8).

In our node classification tasks, we set $L = 2$ and let n_c be the number of classes. After the two convolutional layers, we unwind the complex $N \times F_2$ matrix $\mathbf{X}^{(2)}$ into a real-valued $N \times 2F_2$ matrix, apply a linear layer, consisting of right-multiplication by a $2F_2 \times n_c$ weight matrix $\mathbf{W}^{(3)}$, and then apply softmax. Therefore, our network is given by

$$\text{softmax}(\text{unwind}(\mathbf{Z}^{(2)} (\mathbf{Z}^{(1)} (\mathbf{X}^{(0)}))) \mathbf{W}^{(3)}).$$

For link-prediction, we apply the same method through the unwind layer, but then subtract the rows corresponding to pairs of nodes to obtain the edge features. Figure 3 illustrates the node classification version of MagNet.

4. Related Work

MagNet is related to two research threads in the graph theory literature. In Section 4.1 we describe other graph neural networks designed specifically for directed graphs. Notably, none of these methods encode directionality with complex numbers, instead opting for real-valued, symmetric matrices that are different than the standard graph Laplacian. In doing so, these methods are often more complicated than MagNet. On the other hand, the magnetic Laplacian has been studied for several decades and lately has garnered interest in the network science and graph signal processing communities. However, to the best of our knowledge, this is the first work to use it to construct a graph neural network.

4.1. Neural Networks for Directed Graphs

In Ma et al. (2019), the authors construct a matrix, which they refer to as the directed Laplacian, via identities involving the random walk matrix \mathbf{P} and its stationary distribution $\mathbf{\Pi}$. When G is an undirected graph, one can use the fact that $\mathbf{\Pi}$ is proportional to the degree vector to verify that this matrix reduces to the standard normalized graph Laplacian.

Tong et al. (2020b) use a first-order proximity matrix \mathbf{A}_F , which is merely the symmetrization of the original adjacency matrix, as well as two second-order proximity matrices $\mathbf{A}_{S_{\text{in}}}$ and $\mathbf{A}_{S_{\text{out}}}$. $\mathbf{A}_{S_{\text{in}}}$ is defined by $\mathbf{A}_{S_{\text{in}}}(i, j) \neq 0$ if there exists a k such that $(k, i), (k, j) \in E$, and $\mathbf{A}_{S_{\text{out}}}$ is defined analogously. The authors then construct three different Laplacians and use a fusion operator to share information across channels. Similarly, inspired by Benson et al. (2016), in Monti et al. (2018), the authors consider several different symmetric Laplace matrices corresponding to a number of different graph motifs, i.e., small directed subgraphs representing different connectivity patterns.

Tong et al. (2020a) builds upon the ideas of both Ma et al. (2019) and Tong et al. (2020b) and considers a directed Laplacian similar to the one used in Ma et al. (2019), but with a PageRank matrix in place of the random-walk matrix. This allows for applications to graphs which are not strongly connected. Similar to Tong et al. (2020b), they use higher-order receptive fields (analogous to the second-order adjacency matrices discussed above) and an inception module to share information between receptive fields of different orders. We also note Klicpera et al. (2019), which uses an approach based on PageRank in the spatial domain.

4.2. Related Work on the Magnetic Laplacian and Hermitian Adjacency Matrices

The magnetic Laplacian has been studied since at least Lieb & Loss (1993). The name originates from the interpretation of $\mathbf{L}_U^{(q)}$ as a discrete quantum mechanical Hamiltonian of a charged particle under magnetic flux. Early works focus on

d -regular graphs, settings in which the eigenvectors of the magnetic Laplacian are equivalent to those of the Hermitian adjacency matrix. Such works, therefore, study properties of both matrices (although slightly varied definitions of $\mathbf{H}^{(q)}$ appear). Guo & Mohar (2017), for example, show that using a complex-valued Hermitian adjacency matrix rather than the symmetrized adjacency matrix reduces the number of non-isomorphic cospectral graphs when the number of vertices is small. Topics of current research into the Hermitian adjacency matrices include clustering tasks (Cucuringu et al., 2020) and the role of the parameter q (Mohar, 2020).

The magnetic Laplacian is also the subject of ongoing research in graph signal processing (Furutani et al., 2020), community detection (Fanuel et al., 2017), and clustering (Cloninger, 2017; Fanuel et al., 2018; F. de Resende & F. Costa, 2020). For example, Fanuel et al. (2018) use the phase of the eigenvectors to construct eigenmap embeddings analogous to (Belkin & Niyogi, 2003). In contrast to the graph Laplacian, eigenvalues of the magnetic Laplacian cannot be interpreted as frequencies in an obvious way. Still, spectral properties of the magnetic Laplacian encode graph structural information. Fanuel et al. (2018) show it is unitarily equivalent to the graph Laplacian on the undirected graph if the underlying topology is a tree. In this case, no directional information is captured by the eigenvalues. However, this information may still be encoded by the phase of the eigenvectors (see also Example 1).

The role of q is highlighted in the works of Fanuel et al. (2018), Fanuel et al. (2017) (as well as Guo & Mohar (2017) and Mohar (2020) in the context of the Hermitian adjacency matrix), which show how particular choices of q may highlight various graph motifs. In our context, this indicates that q should be carefully tuned via cross-validation. Lastly, we note that numerous other directed graph Laplacians and Hermitian adjacency matrices, e.g., Chung (2005) and (Chung & Kempton, 2013), have been studied.

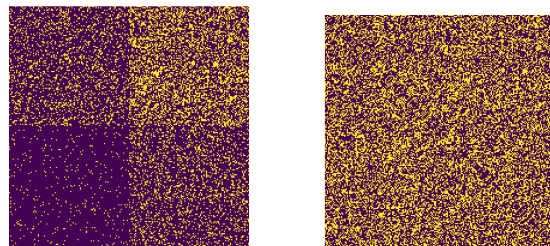
5. Numerical Experiments

We test the performance of MagNet for node classification and link prediction on a variety of benchmark data sets as well as a directed stochastic block model.

5.1. Data Sets

5.1.1. DIRECTED STOCHASTIC BLOCK MODEL

We construct a directed stochastic block model as follows. First we divide N vertices into n_c clusters C_1, \dots, C_{n_c} . To do so, define $\{\alpha_{i,j}\}_{1 \leq i,j \leq n_c}$ to be a collection of probabilities such that $0 < \alpha_{i,j} \leq 1$ with $\alpha_{i,j} = \alpha_{j,i}$, and for an unordered pair $u \neq v$ create an undirected edge between u and v with probability $\alpha_{i,j}$ if $u \in C_i, v \in C_j$. To turn this undirected graph into a directed graph, we next define



(a) Directed adjacency (b) Symmetrized adjacency

Figure 4. The asymmetric adjacency matrix (a) and its symmetrized version (b) with $\alpha_{i,j} = .4, \beta_{1,2} = .9, \beta_{i,i} = .5$.

$\{\beta_{i,j}\}_{1 \leq i,j \leq n_c}$ to be a collection of probabilities such that $0 < \beta_{i,j} \leq 1$ and $\beta_{i,j} + \beta_{j,i} = 1$. For each undirected edge $\{u, v\}$, we assign that edge a direction by the rule that the edge points from u to v with probability $\beta_{i,j}$ if $u \in C_i$ and $v \in C_j$, and points from v to u otherwise. We note that if $\alpha_{i,j}$ is constant, then the only way to determine the clusters will be from the directional information (see Figure 4).

The synthetic datasets *Syn1*, *Syn2*, and *Syn3* are constructed from our directed stochastic block model. In all three datasets, we set $N = 2500, n_c = 5, \beta_{i,i} = .5$, and $\alpha_{i,i} = .1$. For $i \neq j$, we set $\alpha_{i,j} = .1, .08$, and $.05$ in *Syn1*, *Syn2*, and *Syn3*, respectively, and in all three data sets we set $\beta_{i,j} = .95$, for $i < j$. The goal is to classify the vertices by cluster. Decreasing $\alpha_{i,j}$ increases the availability of undirected, structural, information for determining the cluster label. However, since the directed probabilities are so disparate ($\beta_{i,j} = 0.95$ versus $\beta_{j,i} = .05$), and since the graph is relatively sparse ($\alpha_{i,i} = .1$), decreasing $\alpha_{i,j}$ actually makes the clustering problem harder for MagNet and other networks which leverage directed information.

Figure 4 shows the asymmetric adjacency matrix \mathbf{A} along with its symmetrized version for our directed stochastic block model with two clusters and constant $\alpha_{i,j}$. The two clusters are clearly visible when looking at the directed adjacency matrix. Indeed, MagNet is able to achieve high levels of accuracy on *Syn1*, *Syn2*, and *Syn3*, as shown in Table 1. However, the clusters become impossible to detect when looking at the symmetrized version of the adjacency matrix. Therefore, any method which relies on symmetrizing the adjacency matrix will be unable to achieve good results.

5.1.2. REAL DATASETS

Texas, *Wisconsin*, and *Cornell* are WebKB datasets and model the links between websites at different universities¹.

¹<http://www.cs.cmu.edu/afs/cs.cmu.edu/project/theo-11/www/wwkb/>

Table 1. Testing accuracy of node classification. The best results are in **bold** and the second best are underlined.

Type	Method	Syn1	Syn2	Syn3	Cornell	Texas	Wisconsin	Cora-ML	Citeseer
	MagNet	99.8%	98.4%	93.8%	84.3%	<u>83.3%</u>	85.7%	79.8%	67.5%
Spectral	ChebNet	19.8%	20.1%	20.2%	79.8%	79.2%	81.6%	80.0%	66.7%
	GCN	70.2%	67.3%	57.4%	59.0%	57.9%	55.9%	82.0%	66.0%
Spatial	APPNP	98.7%	95.9%	<u>90.3%</u>	58.7%	57.0%	51.8%	82.6%	66.9%
	SAGE	19.5%	20.1%	19.7%	<u>80.0%</u>	84.3%	<u>83.1%</u>	<u>82.3%</u>	66.0%
	GIN	54.9%	54.5%	55.2%	57.9%	65.2%	58.2%	78.1%	63.2%
	GAT	42.6%	42.5%	41.4%	57.6%	61.1%	54.1%	81.7%	<u>67.3%</u>
Directed	DGCN	<u>99.1%</u>	<u>97.3%</u>	88.6%	67.3%	71.7%	65.5%	81.3%	66.3%
	DiGraph	80.7%	78.1%	66.5%	66.8%	64.9%	59.6%	79.4%	62.6%

Table 2. Best q for node classification.

	Syn1	Syn2	Syn3	Cornell	Texas	Wisconsin	Cora-ML	Citeseer
q	0.25	0.1	0.25	0.25	0.15	0.05	0.0	0.0

Table 3. Testing accuracy of link prediction. The best results are in **bold** and the second best are underlined.

Type	Method	Cornell	Texas	Wisconsin	Cora	Citeseer	WikiCS	Email	Chameleon	Squirrel
	MagNet	87.6%	<u>85.5%</u>	85.7%	<u>83.8%</u>	77.0%	83.6%	81.9%	97.3%	97.6%
Spectral	ChebNet	82.5%	83.4%	81.1%	75.2%	58.4%	76.6%	79.1%	95.7%	96.7%
	GCN	83.5%	84.9%	80.4%	76.6%	74.5%	80.1%	78.6%	96.7%	96.6%
Spatial	APPNP	84.2%	84.9%	81.3%	78.4%	76.0%	80.3%	78.7%	96.7%	96.6%
	SAGE	86.2%	85.4%	83.7%	83.2%	77.0%	<u>83.3%</u>	81.9%	97.2%	97.6%
	GIN	84.0%	84.8%	82.4%	78.2%	<u>76.6%</u>	79.0%	77.7%	94.1%	92.7%
	GAT	83.7%	83.3%	84.4%	83.2%	76.3%	81.8%	81.9%	97.0%	97.0%
Directed	DGCN	<u>86.9%</u>	86.1%	<u>84.6%</u>	83.9%	76.3%	<u>83.3%</u>	<u>81.4%</u>	<u>97.2%</u>	<u>97.5%</u>
	Digraph	85.5%	84.6%	84.0%	83.4%	<u>76.6%</u>	82.3%	80.7%	96.4%	97.1%

Table 4. Best q for link prediction.

	Cornell	Texas	Wisconsin	Cora	Citeseer	WikiCS	Email	Chameleon	Squirrel
q	0.2	0.15	0.25	0.25	0.25	0.2	0.1/0.15/0.2/0.25	0.25	0.0/0.1/0.15

We use these datasets for both link prediction and node classification with nodes labeled as student, project, course, staff, and faculty in the latter case. The datasets *Chameleon* and *Squirrel* (Rozemberczki et al., 2019) represent links between Wikipedia pages related to chameleons and squirrels; we use these datasets for link prediction. Likewise, *WikiCS* (Mernyei & Cangea, 2020) is a collection of Computer Science articles, which we also use for link prediction. *Cora-ML* and *CiteSeer* are popular citation networks with node labels corresponding to scientific subareas. For node classification, we use the version of *CiteSeer* provided in Bojchevski & Günnemann (2017) and *Cora-ML* which can be found in the same paper. For link prediction we use the variations of *Cora* and *CiteSeer* provided by Getoor (2005) and Rossi & Ahmed (2015). The *Email* dataset (email-Eu-core) (Leskovec & Krevl, 2014), which we use for link

prediction, is constructed based on email data from a European research institution. Further information is given in the supplementary material.

5.1.3. TRAINING/VALIDATION/TEST SPLITS

Our node classification is performed in a semi-supervised setting (i.e., access to the test data, but not the test labels, during training). For *Cornell*, *Texas*, and *Wisconsin* we use a 60%/20%/20% training/validation/test split, which might be viewed as more akin to supervised learning, because of the small graph size. For all other datasets, we use a small number of training and validation nodes compared to the number of test nodes. For link prediction, we remove 40% of the edges for testing, except for *WikiCS*, where we remove 80% of the edges for testing because of the larger

graph size. Full details are provided in the supplementary material.

5.2. Implementation Details

In all experiments, we used the normalized magnetic Laplacian and implement MagNet with convolution defined as in (6), which means that our network may be viewed as the magnetic Laplacian generalization of ChebNet. We compare with multiple baselines in three categories: (i) spectral methods: ChebNet (Defferrard et al., 2016), GCN (Kipf & Welling, 2016); (ii) spatial methods: APPNP (Klicpera et al., 2019), SAGE (Hamilton et al., 2017), GIN (Xu et al., 2018), GAT (Veličković et al., 2018); and (iii) methods designed for directed graphs: DGCN (Tong et al., 2020b), DiGraph (Tong et al., 2020a). All baselines in the experiments have two graph convolutional layers and one fully connected layer. For ChebNet, we use the symmetrized adjacency matrix. For the spatial networks we apply both the symmetrized and asymmetric adjacency matrix. The results reported in Table 1 are the better of the two results. Full details are provided in the supplementary material. We use Adam as the optimizer and ℓ^2 regularization with the hyperparameter set as $5e^{-4}$ to avoid overfitting. We post the best testing performance by grid-searching based on validation accuracy. For node classification on the synthetic datasets, we generate a one-dimensional node feature sampled from the standard normal distribution. We use the original features for the other node classification datasets. For link prediction, we use the in-degree and out-degree as the node features for all datasets instead the original features. This allows all models to learn directed information from the adjacency matrix. Further details on our training and implementation are given in the supplementary material.

5.3. Results

We see that our network, MagNet, performs well across all tasks. As indicated in Table 2, our cross-validation procedure selects $q = 0$ for node classification on the citation networks *Cora-ML* and *Citeseer* in which case our network essentially reduces to ChebNet. This means we achieved the best performance when regarding directional information as noise, suggesting methods relying on adjacency matrix symmetrization are appropriate in the context of node classification on highly homophilous networks such as citation networks. Indeed, it seems intuitive that $q = 0$ is a good choice in these cases, where the task is to classify research papers by scientific subarea. If the topic of a given paper is “machine learning” then it is likely to both cite other machine learning papers and to be cited by other machine learning papers. For all other datasets, we find that the optimal value of q is nonzero, indicating that directional information is important. Our network exhibits the best performance on five out of six of these datasets and is a close second on

Texas. We also achieve an at least four percentage point improvement over both ChebNet and GCN on all six of these datasets. These networks are quite similar to ours but with the classical (normalized or unnormalized) graph Laplacian rather than the magnetic Laplacian. This isolates the effects of the magnetic Laplacian and shows that it is a valuable tool for encoding directional information when using spectral networks.

MagNet also compares favorably to non-spectral methods on the WebKB networks (*Cornell*, *Texas*, *Wisconsin*). Indeed, MagNet obtains a $\sim 4\%$ improvement on *Cornell* and a $\sim 2.5\%$ improvement on *Wisconsin*, while on *Texas* it has the second best accuracy, close behind SAGE. We also see the other directed methods have relatively poor performance on the WebKB networks, perhaps since these graphs are fairly small and thus have very few training samples.

On the synthetic data sets (*Syn1*, *Syn2*, *Syn3*) we see that methods designed specifically for directed graphs, along with APPNP, do the best. As Figure 4 illustrates, the class label of each vertex depends strongly on the directed information in the graph, and thus methods that cannot extract such information will not perform well.

For link prediction, we achieve the best performance on seven out of nine datasets and are a close second on the other two as shown in Table 3. Moreover, amongst spectral methods, we achieve the best performance on all tasks, often by a significant margin. The next best performance is generally achieved by DGCN. This network relies on second-order directed adjacency matrices (which take $\mathcal{O}(N^3)$ steps to compute) and is also designed specifically for directed graphs. This indicates that incorporating directional information is important for link prediction, even on citation networks such as *Cora* and *CiteSeer* (see also Table 4, which reports optimal non-zero q values for each task). Again, this matches our intuition. There is a clear difference between a paper that is frequently cited and one with many references.

6. Conclusion

We have introduced MagNet, a neural network for directed graphs based on the complex-valued magnetic Laplacian. This network can be viewed as the natural extension of spectral graph convolutional networks to the directed graph setting. We demonstrate the effectiveness of our network, and the importance of incorporating directional information, for both link prediction and node classification tasks on both real and synthetic datasets.

An interesting avenue of future research would include deeper investigation of the role of the charge parameter q . In particular, since different values of q encode different types of directed information, it would be interesting to explore using multiple q ’s along different channels. It

would also be interesting to explore the role of different normalizations of the magnetic Laplacian and to incorporate the magnetic Laplacian into other network architectures.

Acknowledgements

X.Z. and N.B. were funded by the National Institutes of Health (grant #R01GM135929). M.H. acknowledges funding from the National Institutes of Health (grant #R01GM135929), the National Science Foundation (CAREER award #1845856), and the Department of Energy (grant #DE-SC0021152).

A. Github Repository

A Github repository containing code needed to reproduce the results is available at <https://anonymous.4open.science/r/bf901736-c5ac-4b85-ac22-da58960bd8ee/>.

B. List of Method Abbreviations

- MagNet (this paper)
- ChebNet (Defferrard et al., 2016)
- GCN (Kipf & Welling, 2016)
- APPNP (Klicpera et al., 2019)
- GAT (Veličković et al., 2018)
- SAGE (Hamilton et al., 2017)
- GIN (Xu et al., 2018)
- DGCN (Tong et al., 2020b)
- DiGraph (Tong et al., 2020a)

C. Further Implementation Details

We set the parameter $K = 1$ in our implementation of both ChebNet and MagNet. For node classification, we tune the number of filters in [16, 32, 64] for graph convolutional layers and tune the learning rate in $[1e^{-3}, 5e^{-3}, 1e^{-2}]$ for all models. We train all models with a maximum of 3000 epochs and stop early if the validation error doesn't decrease after 500 epochs. One dropout layer with a probability of 0.5 is created before the last linear layer.

Compared with node classification, the number of available samples for link prediction is much larger. Thus, we set a relatively small learning rate of $1e^{-3}$. We train all models with a maximum of 3000 epochs and pick the epoch with the best validation accuracy for testing. We tune the number of filters in [16, 32, 48] for the graph convolutional layers for all models. We do not observe performance improvement by using larger learning rates, dropout, and early stopping in link prediction.

Here are implementation details specific to certain methods:

- We set the parameter ϵ to 0 in GIN for both tasks.
- For GAT, the number of heads tuned in [2, 4, 8].
- For APPNP, we set $K = 10$ for node classification (following the original paper), and search K in [1, 5, 10] for link prediction.
- The coefficient α for PageRank-based models (APPNP, DiGraph) is searched in [0.05, 0.1, 0.15, 0.2].
- DGCN is a bit different than other networks because it requires generating a three-channel Laplacian tensor. For this network, the number of filters is searched in [5, 15, 30] for node classification and [5, 10, 15] for link prediction.
- For DiGraph, the model includes graph convolutional layers without the high-order approximation and inception module.
- For GCN, the normalized directed graph by out-degrees is also tried besides the symmetrized adjacency matrix for both tasks, except for synthetic datasets in node classification since symmetrization will break the cluster pattern. For other spatial methods, including APPNP, GAT, SAGE, and GIN, we also tried both the symmetrized and the original directed graph for two tasks except for synthetic datasets in node classification.

D. Datasets

D.1. Node classification

As shown in Table 5, we use three synthetic datasets and five real datasets for node classification. For citation datasets, *Cora-ML* and *Citeseer*, we randomly select 20 nodes in each class for training, 500 nodes for validation, and the rest for testing following Tong et al. (2020a). For the synthetic datasets (*Syn1*, *Syn2*, *Syn3*), we generate a one-dimensional node feature sampled from the standard normal distribution and randomly select 10 nodes in each cluster for training, 500 nodes for validation, and the rest for testing. Ten folds are generated randomly for each dataset, except for *Cornell*, *Texas* and *Wisconsin*. For *Cornell*, *Texas*, and *Wisconsin*, we use the same training, validation, and testing folds as Pei et al. (2020).

Table 5. Datasets for node classification.

	Syn1	Syn2	Syn3	Cornell	Texas	Wisconsin	Cora-ML	Citeseer
# Nodes	2500	2500	2500	183	183	251	2,995	3,312
# Edges	312,635	261,667	186,984	295	309	499	8,416	4,715
# Features	1	1	1	1,703	1,703	1,703	2,879	3,703
# Classes	5	5	5	5	5	5	7	6

D.2. Link prediction

We use nine real datasets in link prediction as demonstrated in Table 6. Instead of using the original features, we use the in-degree and out-degree as the node features in order to allow the models to learn structural information from the adjacency matrix directly. To construct the datasets that we use for training, validation and testing, which consist of pairs of vertices in the graph, we do the following. If $(u, v) \in E$, we give (u, v) the label 1, otherwise its label is -1. Thus, there are two types of vertex pairs (u, v) with the label -1: (i) $(u, v) \notin E$ but $(v, u) \in E$; and (ii) $(u, v) \notin E$ and $(v, u) \notin E$. The dataset that we use consists of all edges E , all pairs of vertices with label -1 of type (i), and $|E|$ randomly selected pairs of vertices with label -1 of type (ii). For *WikiCS*, the test set consists of 80% of the edges (i.e. vertex pairs with label +1) and 80% of the pairs of vertices with label -1 (randomly selected). For all other datasets, we use 40% instead of 80%, but otherwise the procedure for creating the test data is the same. From within the remaining pairs of vertices, we reserve 20% for validation and the remainder for training. Ten folds are generated for each dataset randomly.

Table 6. Datasets for link prediction.

	Cornell	Texas	Wisconsin	Cora	Citeseer	WikiCS	Email	Chameleon	Squirrel
# Nodes	183	183	251	2,708	3,264	11,701	1,005	2,277	5,201
# Edges	295	309	499	5,429	4,536	216,123	25,571	36,101	217,073
# Features	2	2	2	2	2	2	2	2	2

E. Expanded Tables

Here we present more details on our node classification and link prediction results in Tables 7 and 8. We present our results in the form mean \pm standard deviation. The networks GCN, APPNP, GAT, SAGE, and GIN were not designed with directed graphs as the primary motivation. Therefore, we implemented these methods in two ways: i) with a the original asymmetric adjacency matrix; and ii) with a symmetrized adjacency matrix. For node prediction, symmetrizing the adjacency matrix improved performance for most of these networks on most datasets. For link prediction, on the other hand, using the asymmetric matrix almost always yielded superior results. In our table below, GCN, APPNP, GAT, SAGE, and GIN refer to the implementations with the symmetrized adjacency matrix and GCN-D, APPNP-D, GAT-D, SAGE-D, and GIN-D refer to our implementation with the asymmetric matrix. We did not test the symmetric implementations on our synthetic datasets, *Syn1*, *Syn2*, and *Syn3*, because these datasets, by design, place a heavy importance on directional information.

Table 7. Testing accuracy of node classification. The best results are in **bold** and the second best are underlined.

	Syn1	Syn2	Syn3	Cornell	Texas	Wisconsin	Cora-ML	Citeseer
MagNet	99.8% ±0.1%	98.4% ±0.5%	93.8% ±1.5%	84.3% ±7.0%	83.3%±6.1%	85.7% ±3.2%	79.8%±2.5%	67.5% ±1.8%
ChebNet	19.8%±0.3%	20.1%±0.6%	20.2%±0.8%	79.8%±5.0%	79.2%±7.5%	81.6%±6.3%	80.0%±1.8%	66.7%±1.6%
GCN	-	-	-	59.0%±6.4%	57.9%±5.4%	55.9%±5.4%	82.0%±1.1%	66.0%±1.5%
GCN-D	70.2%±1.3%	67.3%±3.5%	57.4%±1.3%	57.3%±4.8%	58.7%±3.8%	52.7%±5.4%	72.6%±1.6%	60.5%±1.6%
APPNP	-	-	-	58.7%±4.0%	57.0%±4.8%	49.6%±6.5%	82.6% ±1.4%	66.9%±1.8%
APPNP-D	98.7%±0.3%	95.9%±2.1%	<u>90.3%</u> ±1.9%	58.4%±3.0%	56.8%±2.7%	51.8%±7.4%	68.6%±2.5%	58.6%±1.8%
GAT	-	-	-	57.6%±4.9%	61.1%±5.0%	54.1%±4.2%	81.9%±1.0%	67.3%±1.3%
GAT-D	42.6%±6.9%	42.5%±5.4%	41.4%±5.7%	57.3%±7.7%	59.2%±4.1%	52.0%±4.6%	73.1%±1.6%	62.7%±1.6%
SAGE	-	-	-	77.6%±6.3%	84.3% ±5.5%	79.2%±5.3%	82.3%±1.2%	66.0%±1.5%
SAGE-D	19.5%±0.9%	20.1%±0.8%	19.7%±1.1%	80.0%±6.1%	76.2%±3.8%	83.1%±4.8%	72.0%±2.1%	61.8%±2.0%
GIN	-	-	-	57.9%±5.7%	65.2%±6.5%	58.2%±5.1%	78.1%±2.0%	63.3%±2.5%
GIN-D	54.9%±2.6%	54.5%±4.3%	55.2%±3.5%	55.4%±5.2%	58.1%±5.3%	50.2%±7.6%	67.0%±3.2%	60.4%±2.3%
DGCN	99.1%±0.2%	97.3%±0.3%	88.6%±1.1%	67.3%±4.3%	71.7%±7.4%	65.5%±4.7%	81.3%±1.4%	66.3%±2.0%
Digraph	80.7%±2.2%	78.1%±0.8%	66.5%±1.1%	66.8%±6.2%	64.9%±8.1%	59.6%±3.8%	79.4%±1.8%	62.6%±2.2%

 Table 8. Testing accuracy of link prediction. The best results are in **bold** and the second best are underlined.

	Cornell	Texas	Wisconsin	Cora	Citeseer	WikiCS	Email	Chameleon	Squirrel
MagNet	87.6% ±2.6%	85.5%±2.6%	85.7% ±1.9%	83.8%±0.9%	77.0% ±1.3%	83.6% ±0.2%	81.9% ±0.3%	97.3% ±0.1%	97.6% ±0.1%
ChebNet	82.5%±3.0%	83.4%±2.3%	81.1%±2.4%	75.2%±0.5%	58.4%±0.9%	76.6%±0.1%	79.1%±0.3%	95.7%±0.1%	96.7%±0.1%
GCN	75.9%±4.3%	75.7%±2.9%	72.1%±2.1%	74.3%±0.5%	52.9%±0.8%	75.6%±0.1%	78.6%±0.1%	92.8%±1.2%	92.8%±0.4%
GCN-D	83.5%±4.2%	84.9%±2.6%	80.4%±2.3%	76.6%±0.9%	74.5%±2.4%	80.1%±0.2%	78.3%±0.2%	96.7%±0.1%	96.6%±0.1%
APPNP	77.7%±1.7%	77.6%±3.1%	71.1%±3.4%	74.3%±0.7%	53.2%±0.9%	74.9%±0.1%	78.1%±0.1%	91.5%±1.0%	94.8%±0.1%
APPNP-D	84.2%±4.3%	84.9%±2.5%	81.3%±2.2%	78.4%±0.8%	76.0%±2.4%	80.3%±0.2%	78.7%±0.3%	96.7%±0.1%	96.6%±0.1%
GAT	83.7%±2.3%	81.6%±2.0%	81.8%±3.4%	75.8%±0.9%	63.0%±1.7%	72.5%±2.8%	78.8%±0.7%	84.3%±12.1%	88.0%±7.4%
GAT-D	85.8%±3.5%	83.3%±2.5%	84.4%±1.2%	83.2%±0.5%	76.3%±1.8%	81.8%±1.9%	81.9% ±0.2%	97.1%±0.1%	97.0%±0.4%
SAGE	83.6%±2.1%	81.3%±3.1%	81.8%±2.1%	75.7%±0.8%	60.7%±1.5%	76.3%±0.2%	79.3%±0.2%	95.5%±0.2%	96.6%±0.1%
SAGE-D	86.2%±3.9%	85.4%±1.7%	83.7%±1.6%	83.2%±1.0%	77.0% ±1.9%	83.3%±0.1%	81.9% ±0.2%	97.2%±0.1%	97.6% ±0.0%
GIN	74.4%±4.8%	73.5%±3.7%	69.5%±3.3%	73.8%±0.7%	52.9%±1.0%	73.9%±0.5%	77.7%±0.4%	85.0%±2.2%	85.1%±3.7%
GIN-D	84.0%±3.9%	84.8%±2.3%	82.4%±1.9%	78.2%±0.5%	76.6%±2.0%	79.0%±0.1%	76.8%±1.3%	94.1%±1.7%	92.7%±0.2%
DGCN	86.9%±2.8%	86.1% ±1.5%	<u>84.6%</u> ±1.4%	83.9% ±1.0%	76.3%±1.7%	83.3%±0.1%	81.4%±0.2%	97.2%±0.1%	97.5%±0.1%
Digraph	85.5%±3.8%	84.6%±2.2%	84.0%±1.4%	83.4%±0.9%	76.6%±2.4%	82.3%±0.1%	80.7%±0.2%	96.4%±0.1%	97.1%±0.1%

References

- Atwood, J. and Towsley, D. Diffusion-convolutional neural networks. In Lee, D., Sugiyama, M., Luxburg, U., Guyon, I., and Garnett, R. (eds.), *Advances in Neural Information Processing Systems*, volume 29, pp. 1993–2001. Curran Associates, Inc., 2016.
- Belkin, M. and Niyogi, P. Laplacian eigenmaps for dimensionality reduction and data representation. *Neural computation*, 15(6):1373–1396, 2003.
- Benson, A. R., Gleich, D. F., and Leskovec, J. Higher-order organization of complex networks. *Science*, 353(6295):163–166, 2016.
- Bojchevski, A. and Günnemann, S. Deep gaussian embedding of graphs: Unsupervised inductive learning via ranking. In *ICLR Workshop on Representation Learning on Graphs and Manifolds*, 2017.
- Bruna, J., Zaremba, W., Szlam, A., and LeCun, Y. Spectral networks and deep locally connected networks on graphs. In *International Conference on Learning Representations (ICLR)*, 2014.
- Chung, F. Laplacians and the cheeger inequality for directed graphs. *Annals of Combinatorics*, 9(1):1–19, 2005.
- Chung, F. and Kempton, M. A local clustering algorithm for connection graphs. In *International Workshop on Algorithms and Models for the Web-Graph*, pp. 26–43. Springer, 2013.
- Chung, F. R. and Graham, F. C. *Spectral graph theory*. Number 92. American Mathematical Soc., 1997.
- Cloninger, A. A note on markov normalized magnetic eigenmaps. *Applied and Computational Harmonic Analysis*, 43(2): 370 – 380, 2017. ISSN 1063-5203. doi: <https://doi.org/10.1016/j.acha.2016.11.002>.
- Coifman, R. R. and Lafon, S. Diffusion maps. *Applied and computational harmonic analysis*, 21(1):5–30, 2006.
- Cucuringu, M., Li, H., Sun, H., and Zanetti, L. Hermitian matrices for clustering directed graphs: insights and applications. In *International Conference on Artificial Intelligence and Statistics*, pp. 983–992. PMLR, 2020.
- Defferrard, M., Bresson, X., and Vandergheynst, P. Convolutional neural networks on graphs with fast localized spectral filtering. In *Advances in Neural Information Processing Systems 29*, pp. 3844–3852, 2016.
- Duvenaud, D. K., Maclaurin, D., Iparraguirre, J., Bombarell, R., Hirzel, T., Aspuru-Guzik, A., and Adams, R. P. Convolutional networks on graphs for learning molecular fingerprints. In Cortes, C., Lawrence, N., Lee, D., Sugiyama, M., and Garnett, R. (eds.), *Advances in Neural Information Processing Systems*, volume 28, pp. 2224–2232. Curran Associates, Inc., 2015.
- F. de Resende, B. M. and F. Costa, L. d. Characterization and comparison of large directed networks through the spectra of the magnetic laplacian. *Chaos: An Interdisciplinary Journal of Nonlinear Science*, 30(7):073141, 2020.
- Fanuel, M., Alaiz, C. M., and Suykens, J. A. Magnetic eigenmaps for community detection in directed networks. *Physical Review E*, 95(2):022302, 2017.
- Fanuel, M., Alaíz, C. M., Ángela Fernández, and Suykens, J. A. Magnetic eigenmaps for the visualization of directed networks. *Applied and Computational Harmonic Analysis*, 44:189–199, 2018.
- Furutani, S., Shibahara, T., Akiyama, M., Hato, K., and Aida, M. Graph signal processing for directed graphs based on the hermitian laplacian. In *Machine Learning and Knowledge Discovery in Databases*, pp. 447–463, 2020.
- Getoor, L. Link-based classification. In *Advanced methods for knowledge discovery from complex data*, pp. 189–207. Springer, 2005.
- Guo, K. and Mohar, B. Hermitian adjacency matrix of digraphs and mixed graphs. *Journal of Graph Theory*, 85(1):217–248, 2017.
- Hamilton, W. L., Ying, R., and Leskovec, J. Inductive representation learning on large graphs. In *Proceedings of the 31st International Conference on Neural Information Processing Systems, NIPS’17*, pp. 1025–1035, Red Hook, NY, USA, 2017. Curran Associates Inc. ISBN 9781510860964.

- Hammond, D. K., Vandergheynst, P., and Gribonval, R. Wavelets on graphs via spectral graph theory. *Applied and Computational Harmonic Analysis*, 30(2):129–150, 2011.
- Kipf, T. N. and Welling, M. Semi-supervised classification with graph convolutional networks. *arXiv preprint arXiv:1609.02907*, 2016.
- Klicpera, J., Bojchevski, A., and Günnemann, S. Predict then propagate: Graph neural networks meet personalized pagerank. In *ICLR*, 2019.
- Leskovec, J. and Krevl, A. SNAP Datasets: Stanford large network dataset collection. <http://snap.stanford.edu/data>, June 2014.
- Levie, R., Huang, W., Bucci, L., Bronstein, M. M., and Kutyniok, G. Transferability of spectral graph convolutional neural networks. *arXiv preprint arXiv:1907.12972*, 2019.
- Lieb, E. H. and Loss, M. Fluxes, laplacians, and kasteleyn’s theorem. In *Statistical Mechanics*, pp. 457–483. Springer, 1993.
- Ma, Y., Hao, J., Yang, Y., Li, H., Jin, J., and Chen, G. Spectral-based graph convolutional network for directed graphs. *arXiv:1907.08990*, 2019.
- Mernyei, P. and Cangea, C. Wiki-cs: A wikipedia-based benchmark for graph neural networks. *arXiv preprint arXiv:2007.02901*, 2020.
- Mohar, B. A new kind of hermitian matrices for digraphs. *Linear Algebra and its Applications*, 584:343–352, 2020.
- Monti, F., Otness, K., and Bronstein, M. M. Motifnet: A motif-based graph convolutional network for directed graphs. In *2018 IEEE Data Science Workshop*, pp. 225–228, 2018.
- Ortega, A., Frossard, P., Kovačević, J., Moura, J. M., and Vandergheynst, P. Graph signal processing: Overview, challenges, and applications. *Proceedings of the IEEE*, 106(5):808–828, 2018.
- Pei, H., Wei, B., Chang, K. C.-C., Lei, Y., and Yang, B. Geom-gcn: Geometric graph convolutional networks. *arXiv preprint arXiv:2002.05287*, 2020.
- Rossi, R. A. and Ahmed, N. K. The network data repository with interactive graph analytics and visualization. In *AAAI*, 2015. URL <http://networkrepository.com>.
- Rozemberczki, B., Allen, C., and Sarkar, R. Multi-scale attributed node embedding. *arXiv preprint arXiv:1909.13021*, 2019.
- Shi, J. and Malik, J. Normalized cuts and image segmentation. In *Proceedings of IEEE computer society conference on computer vision and pattern recognition*, pp. 731–737. IEEE, 1997.
- Spielman, D. A. and Teng, S.-H. Nearly-linear time algorithms for graph partitioning, graph sparsification, and solving linear systems. In *Proceedings of the thirty-sixth annual ACM symposium on Theory of computing*, pp. 81–90, 2004.
- Tong, Z., Liang, Y., Sun, C., Li, X., Rosenblum, D. S., and Lim, A. Digraph inception convolutional networks. In *NeurIPS*, 2020a.
- Tong, Z., Liang, Y., Sun, C., Rosenblum, D. S., and Lim, A. Directed graph convolutional network. *arXiv preprint arXiv:2004.13970*, 2020b.
- Veličković, P., Cucurull, G., Casanova, A., Romero, A., Liò, P., and Bengio, Y. Graph Attention Networks. *International Conference on Learning Representations*, 2018. URL <https://openreview.net/forum?id=rJXMpikCZ>.
- Wu, Z., Pan, S., Chen, F., Long, G., Zhang, C., and Yu, P. S. A comprehensive survey on graph neural networks. *IEEE Transactions on Neural Networks and Learning Systems*, 32(1):4–24, 2020.
- Xu, K., Hu, W., Leskovec, J., and Jegelka, S. How powerful are graph neural networks? *arXiv preprint arXiv:1810.00826*, 2018.
- Zhou, J., Cui, G., Zhang, Z., Yang, C., Liu, Z., Wang, L., Li, C., and Sun, M. Graph neural networks: A review of methods and applications. *arXiv preprint arXiv:1812.08434*, 2018.